Dual-level reaction-path dynamics (the III approach to VTST with semiclassical tunneling). Application to OH + NH3 → H2O + NH2

ARTICLE · JANUARY 1995

CITATIONS
20

READS
17

5 AUTHORS, INCLUDING:

Jose C Corchado
Universidad de Extremadura
118 PUBLICATIONS **3,304** CITATIONS
SEE PROFILE

Joaquin Espinosa-Garcia
Universidad de Extremadura
141 PUBLICATIONS **2,191** CITATIONS
SEE PROFILE

Wei-Ping Hu
National Chung Cheng University
80 PUBLICATIONS **1,551** CITATIONS
SEE PROFILE

Ivan Rossi
Biodec
73 PUBLICATIONS **1,267** CITATIONS
SEE PROFILE

Dual-Level Reaction-Path Dynamics (the /// Approach to VTST with Semiclassical Tunneling). Application to $OH + NH_3 \rightarrow H_2O + NH_2$

Jose C. Corchado† and Joaquin Espinosa-Garcia

Departamento de Quimica-Fisica, Universidad de Extremadura, 06071-Badajoz, Spain

Wei-Ping Hu, Ivan Rossi, and Donald G. Truhlar*

Department of Chemistry and Supercomputer Institute, University of Minnesota, Minneapolis, Minnesota 55455

Received: August 12, 1994; In Final Form: October 24, 1994®

We consider a new approach to reaction-path dynamics calculations in which the reaction path is calculated at a low level (LL) of theory and stationary point information from a high level (HL) of theory is used to interpolate corrections to energetic quantities, vibrational frequencies, and moments of inertia. Such a calculation is labeled X///Y, where X denotes the high level and Y the low level. The theory is applied to the reaction $OH + NH_3$ and three isotopomeric analogs. The highest-level optimization reported for the saddle point is QCISD(T)//MP2/aug-cc-pVTZ, which yields a classical barrier height of 3.65 kcal/mol. The rate constant is calculated at two levels, QCISD(T)//MP2/aug-cc-pVTZ[MP2/aug-cc-pVDZ]///MP2/6-31G** and QCISD(T)//MP2/aug-cc-pVTZ[MP2/aug-cc-pVDZ]///PM3-SRP; the calculated rate constant for the unsubstituted reaction is approximately invariant to the low level used in the dual-level scheme and agrees with experiment within a factor of 1.13 at 250 K and within a factor of 1.14 at 1500 K.

1. Introduction

In recent papers, direct dynamics calculations based on variational transition state theory[1−3] (VTST) and semiclassical tunneling methods[2,3] have been shown to provide a practical approach to the calculation of chemical reaction rates and to achieving a greater understanding of dynamical bottlenecks, tunneling mechanisms, and kinetic isotope effects in chemical reactions.[4−21] Direct dynamics is the approach by which dynamics calculations are based directly on the output (energies, gradients, and hessians) of electronic structure calculations, without the intermediary of an analytic fit to the potential energy surface. Their strength is the avoidance of the worker-hour-intensive fit step; their weakness is a fairly high cost in terms of computer time because so many electronic structure calculations are involved. The latter cost is minimized compared to full quantal dynamics by the reaction-path approach[22−25] inherent in practical VTST and by the description of tunneling in terms of localized paths[26,27] in semiclassical methods.

In some calculations, in order to ameliorate the cost, semiempirical molecular orbital theory has been used for the electronic structure calculations. Both general parametrizations (such as MNDO,[28] AM1,[29] and PM3[30]) and specific reaction parameters[8,10,14,16] (SRP) have been used. Better accuracy has been achieved by incorporating interpolated corrections[16] (VTST-IC) based on calculations employing higher-level electronic structure theory at selected points on the reaction path. The VTST-IC approach is particularly powerful in that it can be applied even in the wide reaction-swath region[6,31] of geometries accessed by tunneling paths when reaction-path curvature is large.[2,3,27,31,32] This swath is wider than the region that can be represented by an expansion in powers of generalized normal-mode coordinates referenced to the minimum-energy path.

In the present paper we apply this approach to the combustion reaction

$$OH + NH_3 \rightarrow H_2O + NH_2 \qquad (R1)$$

for temperatures in the range 250−2000 K. We also calculated the rate constants of three isotopomeric analogs of this reaction, in particular,

$$OD + NH_3 \rightarrow HDO + NH_2 \qquad (R2)$$

$$OH + ND_3 \rightarrow HDO + ND_2 \qquad (R3)$$

$$OD + ND_3 \rightarrow D_2O + ND_2 \qquad (R4)$$

We also compute kinetic isotope effects (KIEs) as ratios of rate constants for (R1) to those for (R2)−(R4).

The importance of reaction R1 is a consequence of the abundance and reactivity of ammonia in the atmosphere,[33,34] where it has an important role in acid neutralization processes in precipitation.[35] The reaction of ammonia with hydroxyl radical is the rate-determining step of the gas-phase oxidation of ammonia,[36,37] and it is also the key step in the combustion of nitrogen from fossil fuels.[38] Moreover, the knowledge of hydroxyl radical reactions in general is very important in modeling the chemistry of combustion.[39,40]

Reaction R1 has been studied by several experimental techniques, yielding rate constants for a wide range of temperatures.[41−48] In general, the agreement between the different measurements is very good. There are several theoretical studies of this reaction,[19,49−53] including a VTST calculation[19] of the rate constants.

In this work we performed higher-level electronic structure calculations for the stationary points along the reaction path, and these higher-level data are used together with a PM3-SRP semiempirical potential energy surface and a set of reaction-path data from lower-level *ab initio* electronic structure calculations to perform VTST-IC calculations on the reaction rate constants. Tunneling should be important at lower temperatures

† Visiting scientist, Department of Chemistry, University of Minnesota, Spring 1994.

® Abstract published in *Advance ACS Abstracts,* January 1, 1995.

0022-3654/95/2099-0687$09.00/0

because this reaction involves the transfer of a hydrogen atom, and there is an appreciable barrier.

In the course of these calculations we introduce two modifications and extensions of previous approaches:

(i) In the SRP calculations, we explore the effect of relaxing the arithmetic mean rule[54] for the bonding parameter $\beta_{A/B}$.

(ii) We extend the VTST-IC approach to the case where both the low-level calculations used to compute the reaction path and the high-level calculations used for single-point calculations are based on *ab initio* calculations. This is an important advance as it provides the dynamics analog of the double-slash (//) approach[55] to electronic structure calculations. We therefore call it triple-slash dynamcs. In particular, W//X///Z means that the reaction-path data (and reaction-swath data if large-curvature or optimized multidimensional tunneling calculations are carried out) is calculated at lower-level Z and stationary points are calculated at higher-level W//X. As usual, W//X refers to optimization (and frequencies, if applicable) at level X with single-point energies calculated at higher level W.

We also introduce the convenient notation X[Y], which denotes geometry optimization and energy calculated at level X with frequencies at level Y. (This of course involves a geometry optimization at level Y as an intermediate step in calculating frequencies, but this geometry is replaced by the level-X geometry for further stages.)

Thus, one might have an X[Y]///Z calculation where Y is an intermediate level between X and Z. The full generality of the notation is illustrated by a hypothetical four-level calculation called W//X[Y]///Z. In this calculation, the energies for interpolated corrections are obtained at the highest-level W, geometries for the W calculation are optimized (and corrections to the low-level moments of inertia are obtained) at level X, frequencies for interpolated corrections are obtained at lower level Y, and the base for the interpolated corrections is a set of reaction-path geometries, moments of inertia, energies, and frequencies at the lowest-level Z. Each of the overall levels W, X, Y, and Z is itself of the form A/B (if *ab initio*) or AM1, PM3, AM1-SRP, PM3-SRP, *etc.* (if semiempirical). In the A/B notation, A denotes level of electron correlation (*e.g.*, MP2, QCISD(T), ...) or lack thereof (*e.g.*, HF), and B denotes the basis set (*e.g.*, 6-31G*, aug-cc-pVTZ, ...). Furthermore A//C/B is shorthand for A/B//C/B. AM1-SRP denotes an SRP calculation in which one or more parameters were varied from the AM1 set of parameters, and PM3−SRP denotes a variation away from the PM3 set. The label NDDO-SRP refers generically to any SRP method based on neglect of diatomic differential overlap; AM1-SRP and PM3-SRP are special cases of NDDO-SRP.

2. Computational Methods

There are five stationary points of interest along the reaction path: the reactant, the reactant complex, the saddle point, the product complex, and the product. The geometries of these stationary points were optimized, and the harmonic vibrational frequencies of these stationary points were calculated using Dunning's[56,57] augmented correlation consistent polarized valence double zeta (aug-cc-pVDZ) basis sets at the Møller−Plesset[58] second-order perturbation theory (MP2[55]) level. The geometries of the reactant, product, and the saddle point were also optimized with Dunning's[56,57] augmented correlation consistent polarized valence triple zeta (aug-cc-pVTZ) basis set at MP2 levels, and the reactant and product were also optimized with this basis set at the level of quadratic configuration interaction with single and double substitutions and perturbative inclusion of connected triple substitutions [QCISD(T)].[59] In all cases the core electrons were not correlated. These calculations were carried out with the GAUSSIAN 92 program,[60] and they constitute the high level. In this paper, when we say MP2 for a species with an odd number of electrons, we always mean unrestricted MP2 (UMP2[55]). Similarly, QCISD(T) denotes unrestricted QCISD(T).

We performed calculations using both conventional transition state theory[61] (TST) and VTST. The level of VTST we used in this paper is canonical variational theory[1-3] (CVT). In performing the VTST-IC calculations, one uses a low-level surface to obtain data at many points for the dynamics calculations, and then one corrects these data with higher-level results at a small number of points (three with the current algorithm) by interpolation.[16] We performed two sets of dynamics calculations using a different low level in each.

For the low level of the first set of dynamics calculations, we started with the PM3 general parametrization and then adjusted six of the semiempirical parameters to achieve a better representation of critical regions of the potential energy surface, in particular, of the geometries and relative energies of those stationary points. The NDDO-SRP procedure used in this paper is different from that discussed in previous papers. In standard NDDO-derived methods the so-called one-electron resonance integral of NDDO theory is calculated as the overlap integral of two atomic orbitals times a scaling factor, called $\beta_{A/B}$, which is defined as the mean of two atomic β parameters. In the present work we allow some of the $\beta_{A/B}$ to vary independently, and we do *not* require $\beta_{A/B} = {}^1/_2\,(\beta_A + \beta_B)$. We adjusted U_{ss} for N, β_{sHsN}, β_{sHpN}, β_{sHsO}, β_{sHpO}, and β_{pNpO} from their default values. The adjusted values of the six parameters are given in the supplementary material, and the adjustment process is discussed in section 4. Vibrational frequency calculations were also performed on the resulting (PM3-SRP) surface, and the reaction path[62,63] was calculated using the Page−McIver method.[64]

For the low level of the second set of calculations we used reaction-path data calculated at the MP2/6-31G** *ab initio* level[55] in a previous[19] study.

Vibrational frequencies along the reaction path were calculated using Cartesian coordinates.[2,65,66] VTST-IC reaction rate constant calculations were carried out with the POLYRATE version 6.2[67] and MORATE version 6.2[68] programs. The most complete level of tunneling calculation we employed is the microcanonical optimized multidimensional tunneling (μOMT) method,[14] in which—at each energy—the transmission probability is taken as the maximum of two trial calculations, namely, a small-curvature tunneling (SCT) calculation, based on the centrifugal-dominant small-curvature semiclassical adiabatic ground-state approximation (CD-SCSAG),[12,69] and a large-curvature tunneling (LCT) calculation, based on the large-curvature ground-state approximation, version 3 (LCG3).[14,69,70]

Because the standard abbreviations for levels of electron correlation and basis sets are very lengthy, in the rest of the paper we introduce shorthands for the specific levels used in this work, as follows:

PM3-SRP → SRP

MP2/6-31G** → PDZ

MP2/aug-cc-pVDZ → PDZ+

MP2/aug-cc-pVTZ → PTZ+

QCISD(T)//MP2/aug-cc-pVTZ[MP2/aug-cc-pVDZ] → QCIT//PTZ+[PDZ+]

TABLE 1: Geometries of Reactants and Products Calculated at the QCISD(T)/aug-cc-pVTZ Level

	$NH_3(C_{3v})$	$NH_2(C_{2v})$		$H_2O(C_{2v})$	OH
R_{N-H}, Å	1.0152	1.0279	R_{O-H}, Å	0.9619	0.9735
	(1.012)[a]	(1.02)[a]		(0.9576)[b]	(0.9706)[a]
$\angle_{H-N-H}$, deg	106.38	102.86	$\angle_{H-O-H}$, deg	104.20	
	(106.7)[a]	(103.4)[a]		(104.48)[b]	

[a] Experimental value from ref 71. [b] Experimental value from ref 72.

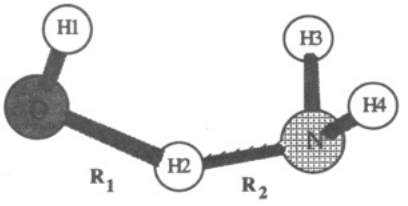

Figure 1. Geometry of the saddle point.

TABLE 2: Geometry[a] of Saddle Point, Reactants, and Products Calculated at Three Levels

	PM3-SRP	MP2/6-31G**	MP2/aug-cc-pVTZ
		Saddle Point	
R_1	1.3056	1.3105	1.3174
R_2	1.0723	1.1097	1.1066
R_{O-H1}	0.9830	0.9688	0.9672
R_{N-H3}	0.9710	1.0154	1.0161
R_{N-H4}	0.9710	1.0154	1.0165
$\angle_{H1-O-H2}$	95.64	103.60	106.13
$\angle_{O-H2-N}$	136.75	141.50	147.78
$\angle_{H3-N-H4}$	110.75	106.01	106.76
		Reactants	
R_2	0.9769	1.0116	1.0122
R_{O-H}	0.9466	0.9712	0.9694
R_{N-H}	0.9769	1.0116	1.0122
$\angle_{H-N-H}$	109.47	106.08	106.78
		Products	
R_1	0.9947	0.9610	0.9615
$\angle_{H-O-H}$	96.93	103.84	104.15
R_{N-H3}	0.9637	1.0233	1.0223
R_{N-H4}	0.9637	1.0233	1.0223
$\angle_{H-N-H}$	112.21	102.75	103.21

[a] See Figure 1 for the atom labeling scheme, and see Table S1 in the supplementary material for the complete geometries in Cartesian coordinates. Bond distances are in Å and angles in deg.

QCISD(T)//MP2/aug-cc-pVTZ → QCIT//PTZ+

QCISD(T)/aug-cc-pVTZ → QCIT/PTZ+

We use the short forms in the text and Tables 4−9 and 11−13 and the long forms in Tables 1−3 and in the figure captions. The reader should recall, however, when reading this shorthand that the PDZ+ basis used here differs from the PDZ basis not only in the addition of diffuse functions but also in having better optimized valence and core functions and a more complete polarization space.[56] The number of contracted basis functions in the PM3, PDZ, PDZ+, and PTZ+ basis sets for the NH_3OH complex is 12, 50, 82, and 184, respectively.

3. Calculations and Results

The optimized geometries calculated for the reactants and products at the QCIT/PTZ+ level are listed and compared to experiment[71,72] in Table 1. The geometry of the saddle point is depicted in Figure 1, and results obtained at various levels are compared in Table 2. The saddle point has C_1 symmetry. The calculated and experimental[73−75] reaction energetics are compared in Table 3. Since the reactant and product complexes (wells in the potential energy surface) are noticeably lower in energy than the reactant and product, respectively, we decided,

TABLE 3: Classical Energies of the Stationary Points along the Reaction Path with Respect to the Reactants in kcal/mol

	reactant well	product well	products	saddle point
PM3	−1.10	−20.75	−17.99	13.70
PM3-SRP	−2.88	−19.20	−14.81	5.89
MP2/6-31G**[a]	−1.32	−15.03	−8.99	9.05
MP2/aug-cc-pVDZ	−1.75	−17.29	−11.87	7.90
PMP2/aug-cc-pVDZ	−1.75	−17.39	−11.96	5.81
MP2/aug-cc-pVTZ			−11.76	4.52
PMP2/aug-cc-pVTZ			−11.82	2.28
QCISD(T)//MP2/aug-cc-pVTZ			−10.08	3.65
QCISD(T)/aug-cc-pVTZ			−10.16	
expt[b]			−9.90	

[a] From ref 19. [b] $\Delta H_f°_0$ from refs 73−75 and zero-point energies from MP2/aug-cc-pVDZ calculations.

TABLE 4: Values of $\langle S^2 \rangle$ of Stationary Points from UHF and UMP2 Calculations

	OH	saddle point
PM3	0.7512	0.7869
SRP	0.7511	0.7802
PDZ+	0.7566	0.7806
PTZ+	0.7571	0.7804
QCIT/PTZ+	0.7573	

following the general guidelines discussed in ref 16, that the interpolated corrections (IC) should be based on these complexes and the saddle point.

For the high-level data, we used the energetics obtained at the QCIT//PTZ+ level and the optimized geometries obtained at the PTZ+ level, and the vibrational frequencies were calculated at the PDZ+ level. We obtained the low-level surface data with two different approaches, namely, the semiempirical SRP approach described in section 2 and the *ab initio* PDZ level presented in ref 19. Thus, the two dynamics levels considered here may be denoted QCIT//PTZ+[PDZ+]///SRP and QCIT//PTZ+[PDZ+]///PDZ, respectively. Note that since we did not carry out QCIT//PTZ+ calculations for the well species, we introduced a further approximation for these species, whose properties are required only for the interpolated corrections, in that we substituted PDZ+ values for the QCIT//PTZ+ energies.

For comparison purposes only, we also performed a few calculations using the spin-projected MP2 method (PMP2).[76] Table 4 gives $\langle S^2 \rangle$ values for the various calculations at stationary points.

The lowest vibrational mode of the generalized transition states is treated as a hindered rotation[14,69,77] in all calculations. All other vibrational modes were treated as harmonic oscillators. In the calculation with the SRP lower level, the four lowest vibrational frequencies along the reaction path are interpolated directly[16,78] (the IVTST-0[78] method) based on the high-level frequencies at the saddle point and the two complexes.

We assume that the electronic excitation energies and degeneracies of the generalized transition state are the same as the conventional transition state one. We assume no low-lying excited states of the ^2A saddle point, and we include the $^2\Pi_{1/2}$ excited state of OH (and OD) in the reactant electronic partition

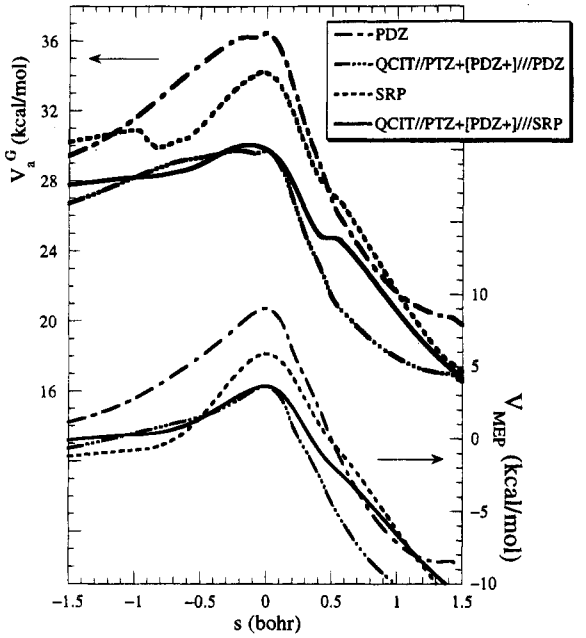

Figure 2. Classical energy profile $V_{MEP}(s)$ (the lower series of curves in the figure) and vibrationally adiabatic ground-state potential curve $V_a^G(s)$ (the top series of curves in the figure) for reaction R1 calculated at different levels. The arrows indicate that the scale for the top is on the left and that for the bottom is on the right.

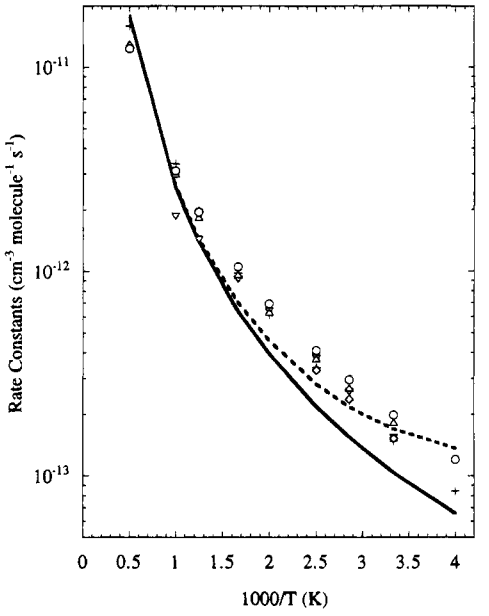

Figure 3. Arrhenius plot of the rate constants of the OH + NH_3 reaction. The solid line denotes CVT/SCT values at the QCISD(T)//MP2/aug-cc-pVTZ[MP2/aug-cc-pVDZ]///MP2/6-31G** level. The dashed line are the CVT/μOMT values at the QCISD(T)//MP2/aug-cc-pVTZ-[MP2/aug-cc-pVDZ]///PM3-SRP level. The symbols are experimental data: ▽, ref 42; +, ref 44; △, ref 45; ○, ref. 46, ◇, ref 48.

function. We use the experimental value,[71] 140 cm^{-1}, for the excitation energy of this state.

Figure 2 shows the classical energy profile $V_{MEP}(s)$ and the vibrationally adiabatic ground-state potential curve $V_a^G(s)$ for reaction R1 calculated at the SRP, PDZ, QCIT//PTZ+[PDZ+]///SRP, and QCIT//PTZ+///PDZ levels, where s is the reaction coordinate. The vibrational adiabatic ground-state potential curve for a bimolecular reaction is obtained by adding the local zero point energy to $V_{MEP}(s)$.

The tunneling contributions are calculated at the ///SRP level using the μOMT method with the reactant and the exit channel for the large-curvature tunneling[69] (LCT) part of the calculation restricted to the vibrational ground state. We checked the importance of tunneling into excited vibrational states of the product in the LCT calculation, and it only changes the final CVT/μOMT rates by less than 10% for R1 and R2 and less than 1% for R3 and R4 at the lowest temperature under study (250 K). So the neglect of the excited-state contribution in the LCT calculations in this study is justified. For the calculation at the ///PDZ level, tunneling contributions are calculated with the SCT method.

The calculated rate constants at different temperatures and some experimental[46] results are summarized in Table 5. Figure 3 shows an Arrhenius plot.

The calculated kinetic isotope effects (KIEs) and the factor analyses[8,79] of the KIEs at different temperatures are listed in Tables 6−10, all at the ///SRP level with μOMT tunneling (our most complete dynamical level). The calculated and experimental[46] activation energies are shown in Table 11. Theoretical activation energies are obtained by two-point Arrhenius fits at the temperatures indicated in the first column, and they represent average values over the corresponding temperature interval, which is the appropriate quantity for comparisons to experiment.

4. Discussion

The calculated geometries of the reactants and products at the QCIT/PTZ+ level are in good agreement with the experimental[71,72] values. The discrepancies in bond lengths are less than 0.01 Å, and the discrepancies in bond angles are less than 0.6°.

An experimental value for the reaction energy was obtained by

$$\Delta E = \Delta H_0 - \text{ZPE(products)} + \text{ZPE(reactants)} \quad (1)$$

where ZPE denotes zero point energy. This value of ΔE is compared to those calculated directly at various levels of electronic structure theory in Table 3. This table shows that the calculated exoergicities are not very sensitive to the basis sets, but they are more sensitive to the level of electron correlation. Our best calculation (QCIT/PTZ+) gives excellent agreement (< 0.3 kcal) with the experimental value.

Table 3 also compares the various calculated classical barrier heights, which are more sensitive to the basis sets and are also sensitive to the level of electron correlation. The barrier is lowered by 5.4 kcal from the PDZ level to the QCIT//PTZ+ level. The present work shows that the PMP2 method tends to overcorrect the energies at the saddle point and results in barriers that are too low for a given basis set.

The PM3 method predicts a reaction energy which is 8.1 kcal too exoergic and a barrier height which is approximately 10 kcal too high. Thus, the PM3 surface is not a good approximation to the true surface, and that is why we calibrated a more accurate one to serve as the first low-level surface in the VTST-IC dynamics calculations. The modified PM3 surface, which is called the PM3-SRP surface or just the SRP surface, reduces the error to about 5 kcal in the exoergicity and to approximately 2 kcal in the barrier height.

The assumption that $\beta_{A'B} = {}^1/_2\,(\beta_{AA} + \beta_{B'B})$ was made in earlier work to reduce the dimensionality of the parameter space and simplify the general parametrization of the method.[28−30,54] Since NDDO-SRP parameters are not meant to be general but instead are determined for a specific reaction under study, we now prefer to relax this arithmetic mean rule, allowing in principle for a different $\beta_{A'B}$ for every type of two-orbital

TABLE 5: Rate Constants of the OH + NH_3 Reaction (in cm^3 $molecule^{-1}$ s^{-1})

	QCIT//PTZ+[PDZ+]	QCIT//PTZ+[PDZ+]///SRP			QCIT//PTZ+[PDZ+]///PDZ		
T (K)	TST	CVT	CVT/SCT	CVT/μOMT	CVT	CVT/SCT	expt[a]
250	1.75(−14)[b]	1.15(−14)	6.78(−14)	1.36(−13)	1.74(−14)	6.55(−14)	1.20(−13)
300	4.16(−14)	3.00(−14)	1.06(−13)	1.69(−13)	4.12(−14)	1.03(−13)	1.98(−13)
400	1.32(−13)	1.07(−13)	2.20(−13)	2.80(−13)	1.31(−13)	2.17(−13)	4.09(−13)
500	2.89(−13)	2.49(−13)	3.97(−13)	4.57(−13)	2.84(−13)	3.92(−13)	6.93(−13)
600	5.23(−13)	4.69(−13)	6.45(−13)	7.07(−13)	5.13(−13)	6.38(−13)	1.05(−12)
800	1.27(−12)	1.18(−12)	1.37(−12)	1.44(−12)	1.24(−12)	1.39(−12)	1.95(−12)
1000	2.46(−12)	2.32(−12)	2.54(−12)	2.62(−12)	2.40(−12)	2.57(−12)	3.11(−12)
1500	7.99(−12)	7.60(−12)	7.85(−12)	7.95(−12)	7.85(−12)	8.04(−12)	7.01(−12)
2000	1.80(−11)	1.70(−11)	1.74(−11)	1.75(−11)	1.76(−11)	1.78(−11)	1.23(−11)

[a] Experimental results from ref 46. [b] 1.75(−14) is an abbreviation for 1.75×10^{-14}.

TABLE 6: Kinetic Isotope Effects[a]

T (K)	k_1/k_2	k_1/k_3	k_1/k_4
250	0.96	10.15	9.32
300	0.93	7.32	6.73
400	0.93	4.64	4.38
500	0.95	3.52	3.39
600	0.98	2.89	2.86
800	0.99	2.21	2.25
1000	1.01	1.91	1.97
1500	1.04	1.57	1.70
2000	1.06	1.45	1.62

[a] Calculated using the CVT/μOMT rate constants at the QCIT//PTZ+[PDZ+]///SRP level.

TABLE 7: Factor Analysis of k_1/k_2[a]

T (K)	$\eta_{vibrational}$	$\eta_{tunneling}$	$\eta_{variational}$
250	0.41	1.30	1.13
300	0.46	1.12	1.11
400	0.51	1.03	1.08
500	0.54	1.01	1.07
600	0.56	1.01	1.06
800	0.58	0.98	1.05
1000	0.59	0.99	1.04
1500	0.61	0.99	1.04
2000	0.62	0.99	1.05

[a] $\eta_{translational}$ and $\eta_{rotational}$ are independent of temperature, and their values are 1.04 and 1.58, respectively.

TABLE 8: Factor Analysis of k_1/k_3[a]

T (K)	$\eta_{vibrational}$	$\eta_{tunneling}$	$\eta_{variational}$
250	4.09	1.53	0.72
300	3.00	1.39	0.78
400	2.00	1.21	0.85
500	1.54	1.13	0.90
600	1.29	1.08	0.93
800	1.01	1.01	0.95
1000	0.88	1.00	0.97
1500	0.72	0.99	0.97
2000	0.66	1.00	0.97

[a] $\eta_{translational}$ and $\eta_{rotational}$ are independent of temperature, and their values are 1.12 and 2.00, respectively.

interaction. The result is that the wave function is more flexible, and it is easier to fit the NDDO potential energy surface to the reference *ab initio* one.

One complication in finding the SRP parameters for reaction R1 is that since the reaction is very exoergic, the conventional transition state is "early", and almost any parameters that lower the barrier height will also lower the energy of the reactant complex. However, the PM3 energy of the complex (relative to the reactant) is already very close to the high-level values (see Table 3), and significantly lowering the energy of the complex by the SRP method would make the reaction path unrealistic. Special care has been taken with the SRP method not to lower the energy of the reactant complex too much, while

TABLE 9: Factor Analysis of k_1/k_4[a]

T (K)	$\eta_{vibrational}$	$\eta_{tunneling}$	$\eta_{variational}$
250	1.60	1.90	0.78
300	1.29	1.61	0.83
400	0.96	1.31	0.88
500	0.79	1.18	0.92
600	0.69	1.13	0.95
800	0.57	1.04	0.97
1000	0.51	1.01	0.98
1500	0.44	1.00	0.99
2000	0.41	1.00	1.00

[a] $\eta_{translational}$ and $\eta_{rotational}$ are independent of temperature, and their values are 1.18 and 3.33, respectively.

TABLE 10: Transitional Mode Contributions to KIEs

T (K)	k_1/k_2	k_1/k_3	k_1/k_4
250	0.46	0.30	0.19
300	0.50	0.34	0.22
400	0.54	0.39	0.26
500	0.57	0.41	0.28
600	0.59	0.43	0.29
800	0.61	0.44	0.31
1000	0.62	0.45	0.32
1500	0.63	0.45	0.33
2000	0.64	0.44	0.33

TABLE 11: Energies of Activation of (R1) in kcal/mol Calculated with Four Dynamics Approximations at the QCIT//PTZ+[PDZ+]///SRP Level and Compared to Experiment

T (K)	TST	CVT	CVT/SCT	CVT/μOMT	expt[a]
250−300	2.58	2.87	1.33	0.66	1.49
400−600	3.28	3.52	2.57	2.21	2.25
800−1000	5.28	5.39	4.90	4.75	3.71
1500−2000	9.66	9.63	9.47	9.41	6.79

[a] Experimental results from ref 46.

we tried to lower the barrier height and decrease the exoergicity. In the adjustment process, the parameters β_{sHsO} and β_{sHpO} were changed primarily for adjusting the barrier height and exoergicity, the parameters β_{sHsN} and β_{sHpN} were changed for lowering the barrier and keeping the reactant complex from being too low in energy, the parameter U_{ss} for N was changed to decrease the high positive charge on the nitrogen atom in the original PM3 parametrization, and the parameter β_{pNpO} was changed for fine-tuning the energetics and geometries.

Figure 2 shows that, when the SRP method is used for the low level, the variational transition state at 0 K, which is the maximum of the vibrationally adiabatic ground-state potential curve, is a little earlier than the saddle point. However, for the ///PDZ calculation, the variational transition state at 0 K is very close to the saddle point.

In Table 5 and Figure 3 we notice that all dynamics calculations that include tunneling agree well with the experimental values in most of the temperature range under study,

especially at higher temperatures. Also, recent experimental measurement by Diau *et al.*[48] using a KrF laser for photolysis indicated that most of the earlier experimental rates might be too high in the 300−400 K temperature range. Our CVT/μOMT results agree very well with their new experimental results over this range (see Figure 2). The CVT/μOMT calculation predicts higher rates than the CVT/SCT calculation at lower temperatures because large-curvature tunneling (LCT) is dominant at lower energies. The reaction-path data from PDZ calculations do not provide enough information to perform an LCT calculation, which requires information from a wider region—called the swath—which cannot be obtained from an expansion around the reaction path, and the best method one can use in that case is the SCT approximation. In the μOMT calculation the LCT mechanism is the dominant tunneling mechanism below 31.3 kcal (relative to the classical energy of the reactant), which is 3.0 kcal below the adiabatic ground-state barrier. (The adiabatic ground-state barrier height relative to the zero point energy of reactants is 5.3 kcal.) Since the representative tunneling energies in μOMT calculations for temperatures above 500 K are above this energy, the use of the SCT approximation is justified at higher temperatures.

The excellent agreement of the ///SRP and ///PDZ levels for the CVT/SCT calculations in Table 5 is one of the major points of this paper. It shows that dual-level techniques are approximately invariant to the low level, as they should be, if the low level is reasonable. The present comparison is quite convincing in this regard since two quite different approaches are used for the lower level.

Table 11 shows that the calculations including tunneling give better agreement (than the TST and CVT calculations) with experimental activation energies at lower temperatures. At higher temperatures all the calculations predict higher activation energies than experiment, and we tentatively attribute this by vibrational anharmonicities which are more severe at higher temperatures or to our barrier height being too high or both.

Table 6 presents the KIEs calculated using the CVT/μOMT rate constants with the NDDO-SRP surface and the IC method. Note that the KIEs are defined as the ratio of the rate constants of (R1) to (R2), (R3), or (R4). This follows the conventional approach in which the rate for the lighter isotope is always in the numerator. With this convention, KIEs and KIE factors greater than one are called "normal", and those less than one are called "inverse".

For (R2), the KIEs are close to unity at all temperatures. Both (R3) and (R4) show significant kinetic isotope effects at lower temperatures, and the KIEs have negative temperature dependences. Superficially, one would think that (R2) has KIEs close to unity because the O−H and O−D vibrations in the reactants of (R1) and (R2) are merely spectator modes throughout the course of reaction. However, from Table 7 we see that it is the result of the balancing between the normal rotational contribution and the inverse vibrational contribution. Detailed analysis (see Table 10) indicates that the inverse vibrational contribution originates from the four transitional modes of the transition states. (A transitional mode is defined as one whose frequency tends to zero in both the reactant and product limits.)

The high normal KIEs of (R3) at low temperatures result primarily from the high vibrational contribution and, to a lesser extent, from the rotational and tunneling contributions. Table 8 shows that the vibrational contribution decreases as the temperature increases and eventually becomes inverse at very high temperatures, and it is responsible for most of the temperature dependence of the KIEs. Detailed analysis shows that the high vibrational contribution at low temperatures and

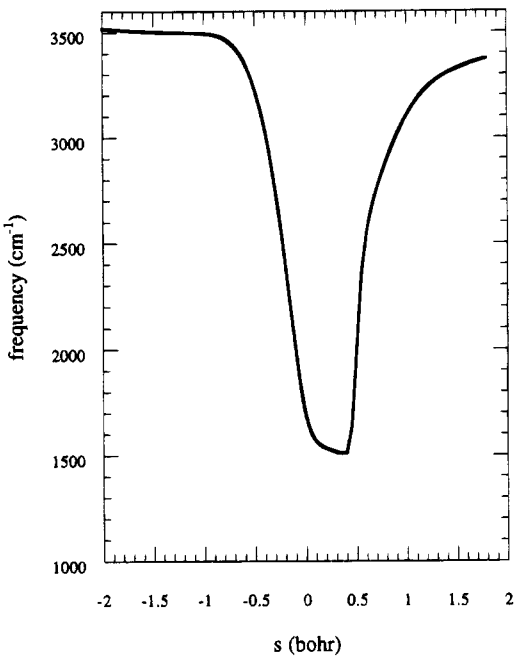

Figure 4. N···H···O symmetric stretching (mode 4) vibrational frequency along the reaction path for reaction R1 calculated at the QCISD(T)//MP2/aug-cc-pVTZ[MP2/aug-cc-pVDZ]///PM3-SRP level.

TABLE 12: Bottleneck Properties for (R1) in the QCIT// PTZ+[PDZ+]///SRP Calculation

T (K)	s_*^{CVT} (a_0)[a]	$V_{MEP}(s_*^{CVT})$[b]	$V_a^G(s_*^{CVT})$[b]	R_1 (Å)[c]	R_2 (Å)[c]
d	0.0000	3.65	29.77	1.306	1.072
0	−0.1305	3.33	30.04	1.374	1.034
250	−0.1192	3.38	30.03	1.369	1.037
300	−0.1051	3.43	30.02	1.361	1.041
400	−0.0938	3.47	30.01	1.356	1.044
500	−0.0924	3.48	30.01	1.355	1.044
600	−0.0898	3.49	30.00	1.353	1.045
800	−0.0660	3.56	29.97	1.341	1.052
1000	−0.0654	3.56	29.97	1.340	1.052
1500	−0.0656	3.56	29.97	1.340	1.052
2000	−0.0766	3.53	29.99	1.346	1.048

[a] The scaling mass is 1 a.m.u. [b] In kcal/mol. [c] PM3-SRP geometry; see Figure 1 for definition of R_1 and R_2. [d] Saddle point property.

the temperature dependence of the contribution originate primarily from a mode that corresponds to stretching between the nitrogen atom and the hydrogen atom that is abstracted by the hydroxyl radical. The vibrational frequency of this mode along the reaction path for (R1) is shown in Figure 4. Since this isotopically sensitive frequency decreases on proceeding from the reactant to the transition state, it contributes significantly to the normal KIEs. The bending modes of ND_3 also contribute to the normal KIEs. The tunneling contribution, as expected, decreases as temperature increases and approaches unity at high temperatures. It is also noted that the tunneling contribution for KIEs is higher in the (R3) case than for (R2) because the atom being transferred is hydrogen in both (R1) and (R2) and is deuterium in (R3). The variational contribution is close to unity for k_1/k_2, and it is inverse for k_1/k_3 and k_1/k_4 with a slightly positive temperature dependence in the temperature range under study. The bottleneck properties for (R1) and (R2) are shown in Tables 12 and 13. Both (R3) and (R4) have much smaller variational effects. (A "variational effect" is the difference between CVT and TST.) The translational and rotational contributions are normal, and they are temperature independent. The contributions for the KIEs of (R4) are just the combined effects of those in (R2) and (R3), and the resulting KIEs turn out to be very similar to (R3). The lower vibrational

TABLE 13: Bottleneck Properties for (R2) in the QCIT// PTZ+[PDZ+]///SRP Calculation

T (K)	s_*^{CVT} (a_0)[a]	$V_{MEP}(s_*^{CVT})$[b]	$V_a^G(s_*^{CVT})$[b]	R_1 (Å)[c]	R_2 (Å)[c]
d	0.0000	3.65	27.96	1.306	1.072
0	−0.1405	3.21	28.28	1.379	1.032
250	−0.1228	3.31	28.28	1.370	1.036
300	−0.1157	3.34	28.28	1.367	1.038
400	−0.1050	3.39	28.27	1.361	1.041
500	−0.1036	3.40	28.27	1.360	1.041
600	−0.0908	3.45	28.25	1.353	1.045
800	−0.0818	3.49	28.24	1.349	1.047
1000	−0.0811	3.49	28.24	1.349	1.047
1500	−0.0853	3.47	28.24	1.351	1.046
2000	−0.1032	3.40	28.27	1.360	1.041

[a] The scaling mass is 1 amu. [b] In kcal/mol. [c] PM3-SRP geometry; see Figure 1 for definition of R_1 and R_2. [d] Saddle point property.

contribution compared to (R3) is because of more inverse contribution from the four transitional modes.

The most expensive steps in the QCIT//PTZ+[PDZ+]///SRP and QCIT//PTZ+[PDZ+]///PDZ calculations in this work are the saddle point geometry optimization at PTZ+ level and the single point calculation at the QCIT level with the PTZ+ geometry. Since an accurate barrier height is essential for the dynamics calculations, and it is especially critical for tunneling-dominated reactions at low temperatures, the emphasis on using available computing resources for determining the barrier height is well justified.

5. Concluding Remarks

We have demonstrated the practicality of dual-level dynamics calculations in which the reaction-path information is calculated at a low level of *ab initio* theory, and limited stationary point information is incorporated at a higher level. We also test the importance of including information from the wider reaction-swath region by a calculation in which semiempirical molecular orbital theory is used for the lower-level calculation. The introduction of such dual-level techniques into the direct dynamics method is expected to play a significant role in future applications of electronic structure theory to chemical kinetics because it allows variational transition state theory and semiclassical tunneling calculations to be employed with approximately the same amount of high-level electronic structure data as is required for conventional transition state theory.

Three sets of kinetic isotope effects (KIEs) have been predicted over a wide temperature range in this work. Any future experimental studies of these KIEs will be valuable in evaluating the success of the theory.

Acknowledgment. The authors are grateful to Rozeanne Steckler for continuing collaboration on the interface of electronic structure methods with reaction-path dynamics. Our work on VTST is supported in part by the U.S. Department of Energy, Office of Basic Energy Sciences. Additional support for high-energy chemical reactions is provided by NASA.

Supplementary Material Available: Tables of geometries, SRP parameters, and vibrational frequencies (4 pages). Ordering information is given on any current masthead page.

References and Notes

(1) Truhlar, D. G.; Garrett, B. C. *Acc. Chem. Res.* **1980**, *13*, 440.
(2) Truhlar, D. G.; Isaacson, A. D.; Garrett, B. C. In *Theory of Chemical Reaction Dynamics*; Baer, M., Ed.; CRC Press: Boca Raton, 1985; Vol. 4, p 65.
(3) Truhlar, D. G.; Garrett, B. C. *Annu. Rev. Phys. Chem.* **1984**, *35*, 159.
(4) Doubleday, C., Jr.; McIver, J. W., Jr.; Page, M. *J. Phys. Chem.* **1988**, *92*, 4367.
(5) Baldridge, K. K.; Gordon, M. S.; Steckler, R.; Truhlar, D. G. *J. Phys. Chem.* **1989**, *93*, 5107.
(6) Truhlar, D. G.; Gordon, M. S. *Science* **1990**, *249*, 491.
(7) Garrett, B. C.; Koszykowski, M. L.; Melius, C. F.; Page, M. *J. Phys. Chem.* **1990**, *94*, 7096.
(8) Gonzalez-Lafont, A.; Truong, T. N.; Truhlar, D. G. *J. Phys. Chem.* **1991**, *95*, 4618.
(9) Truong, T. N.; McCammon, J. A. *J. Am. Chem. Soc.* **1991**, *113*, 7504.
(10) Viggiano, A. A.; Paschkewitz, J.; Morris, R. A.; Paulson, J. F.; Gonzalez-Lafont, A.; Truhlar, D. G. *J. Am. Chem. Soc.* **1991**, *113*, 9404.
(11) Garrett, B. C.; Melius, C. F. In *Theoretical and Computational Models for Organic Chemistry*; Formosinho, S. J., Csizmadia, I. G., Arnaut, L. G., Eds.; Kluwer: Dordrecht, 1991; p 35.
(12) Liu, Y.-P.; Lynch, G. C.; Truong, T. N.; Lu, D.-h.; Truhlar, D. G. *J. Am. Chem. Soc.* **1993**, *115*, 2408.
(13) Isaacson, A. D.; Wang, L.; Scheiner, S. *J. Phys. Chem.* **1993**, *97*, 1765.
(14) Liu, Y.-P.; Lu, D.-h.; Gonzalez-Lafont, A.; Truhlar, D. G.; Garrett, B. C. *J. Am. Chem. Soc.* **1993**, *115*, 7806.
(15) Storer, J. W.; Houk, K. N. *J. Am. Chem. Soc.* **1993**, *115*, 10426.
(16) Hu, W.-P.; Liu, Y.-P.; Truhlar, D. G. *J. Chem. Soc., Faraday Trans.* **1994**, *90*, 1715.
(17) Truong, T. N. *J. Chem. Phys.* **1994**, *100*, 8014.
(18) Espinosa-Garcia, J.; Corchado, J. C. *J. Chem. Phys.* **1994**, *101*, 1333.
(19) Espinosa-Garcia, J.; Corchado, J. C. *J. Chem. Phys.* **1994**, *101*, 8700.
(20) Page, M. *Comput. Phys. Commun.* **1994**, *84*, 115.
(21) The direct dynamics approach may also be applied with other kinds of dynamics, *e.g.*, classical trajectories: (a) Malcome-Lawes, D. J. *J. Chem. Soc., Faraday Trans. 2* **1975**, *71*, 1183. (b) Truhlar, D. G.; Duff, J. W.; Blais, N. C.; Tully, J. C.; Garrett, B. C. *J. Chem. Phys.* **1982**, *77*, 764. (b) Car, R.; Parrinello, M. *Phys. Rev. Lett.* **1985**, *55*, 2471.
(22) Eliason, M. A.; Hirschfelder, J. O. *J. Chem. Phys.* **1959**, *30*, 1426.
(23) Hofacker, L. *Z. Naturforsch. A* **1963**, *18*, 607.
(24) Marcus, R. A. *J. Chem. Phys.* **1966**, *45*, 4493.
(25) Truhlar, D. G. *J. Chem. Phys.* **1970**, *53*, 2041.
(26) Marcus, R. A.; Coltrin, M. E. *J. Chem. Phys.* **1977**, *67*, 2609.
(27) Truhlar, D. G.; Garrett, B. C. *J. Chim. Phys.* **1987**, *84*, 365.
(28) Dewar, M. J. S.; Thiel, W. *J. Am. Chem. Soc.* **1977**, *99*, 4899.
(29) Dewar, M. J. S.; Zoebisch, E. G.; Healy, E. F.; Stewart, J. J. P. *J. Am. Chem. Soc.* **1985**, *107*, 3902.
(30) Stewart, J. J. P. *J. Comput. Chem.* **1989**, *10*, 221.
(31) (a) Garrett, B. C.; Truhlar, D. G.; Wagner, A. F.; Dunning, T. H., Jr. *J. Chem. Phys.* **1983**, *78*, 4400. (b) Bondi, D. K.; Connor, J. N. L.; Garrett, B. C.; Truhlar, D. G. *J. Chem. Phys.* **1983**, *78*, 5981.
(32) Babamov, V. K.; Marcus, R. A. *J. Chem. Phys.* **1978**, *74*, 1790.
(33) Graedel, T. E. *Chemical Compounds in the Atmosphere*; Academic Press: New York, 1978.
(34) Levy, H. II *Planet. Space Sci.* **1973**, *21*, 575.
(35) Wofsy, S. C.; McElroy, M. B. *Can. J. Chem.* **1974**, *52*, 1582.
(36) McConell, J. C. *J. Geophys. Res.* **1973**, *78*, 7812.
(37) Report of the NASA working group on troposphere programm planning; NASA Reference Publication, 1980, p 1062.
(38) Song, Y. H.; Blair, D. W.; Siminski, V. J.; Bartok, W. *Symp. (Int.) Combust., [Proc.], 18th* **1981**, 53.
(39) Baker, R. R.; Baldwin, R. R.; Walker, R. W. *Symp. (Int.) Combust. [Proc.], 13th* **1971**, 291.
(40) Barnard, J. A.; Bradley, J. N. *Flame and Combustion*, 2nd ed.; Chapman and Hall: New York, 1985.
(41) Perry, R. A.; Atkinson, R.; Pitts, J. N., Jr. *J. Chem. Phys.* **1976**, *64*, 3237.
(42) Silver, J. A.; Kolb, C. E. *Chem. Phys. Lett.* **1980**, *75*, 191.
(43) Stephens, R. D. *J. Phys. Chem.* **1984**, *88*, 3308.
(44) Salimian, S.; Hanson, R. K.; Kruger, C. H. *Int. J. Chem. Kinet.* **1984**, *16*, 725.
(45) Zabielski, M. F.; Seery, D. J. *Int. J. Chem. Kinet.* **1985**, *17*, 1191.
(46) Jeffries, J. B; Smith, G. P. *J. Phys. Chem.* **1986**, *90*, 487.
(47) Fujii, N.; Chiba, K.; Uchida, S.; Miyama, H. *Chem. Phys. Lett.* **1986**, *127*, 141.
(48) Diau, E. W.-G.; Tso, T.-L; Lee, Y.-P. *J. Phys. Chem.* **1990**, *94*, 5261.
(49) Leroy, G.; Sana, M.; Tinant, A. *Can. J. Chem.* **1985**, *63*, 1447.
(50) Gimenez, X.; Moreno, M.; Lluch, J. M. *Chem Phys* **1992**, *165*, 41.
(51) Espinosa-Garcia, J.; Corchado, J. C.; Sana, M. *J. Chim. Phys.* **1993**, *90*, 1181.
(52) (a) Corchado, J. C.; Olivares del Valle, F. J.; Espinosa-Garcia, J. *J. Phys. Chem.* **1993**, *97*, 9129. (b) Corchado, J. C.; Olivares del Valle, F. J.; Espinosa-Garcia, J. *J. Phys. Chem.* **1994**, *98*, 5796 (E).
(53) Espinosa-Garcia, J.; Ojalvo, E. A.; Corchado, J. C. *J. Mol. Struct. (THEOCHEM)* **1994**, *303*, 131.

(54) Pople, J. A.; Santry, D. P.; Segal, G. A. *J. Chem. Phys.* **1965**, *43*, S129.

(55) Hehre, W. J.; Radom, L.; Schleyer, P. v. R.; Pople, J. A. *Ab initio Molecular Orbital Theory*; Wiley; New York, 1986.

(56) Dunning, T. H., Jr. *J. Chem. Phys.* **1989**, *90*, 1007.

(57) Kendall, R. A.; Dunning, T. H., Jr.; Harrison, R. J. *J. Chem. Phys.* **1992**, *96*, 6796.

(58) Møller, C.; Plessett, M. S. *Phys. Rev.* **1934**, *46*, 618.

(59) Pople, J. A.; Head-Gordon, M. *J. Chem. Phys.* **1985**, *82*, 284.

(60) GAUSSIAN 92, Revision G.1: Frisch, M. J.; Trucks, G. W.; Schlegel, H. B.; Gill, P. M. W.; Johnson, B. G.; Wong, M. W.; Foresman, J. B.; Robb M. A.; Head-Gordon, M.; Replogle, E. S.; Gomperts, R.; Andres, J. L.; Raghavachari, K.; Binkley, J. S.; Gonzalez, C.; Martin, R. L.; Fox, D. J.; Defrees, D. J.; Baker, J.; Stewart, J. J. P.; Pople, J. A. Gaussian, Inc., Pittsburgh, PA, 1993.

(61) Eyring, H. *J. Chem. Phys.* **1935**, *3*, 107.

(62) Shavitt, I. *J. Chem. Phys.* **1968**, *49*, 4048.

(63) Truhlar, D. G.; Kuppermann, A. *J. Am. Chem. Soc.* **1971**, *93*, 1840.

(64) Page, M.; McIver, J. W. *J. Chem. Phys.* **1988**, *88*, 922.

(65) Miller, W. H.; Handy, N. C.; Adams, J. E. *J. Chem. Phys.* **1980**, *72*, 99.

(66) Natanson, G. A.; Garrett, B. C.; Truong, T. N.; Joseph, T.; Truhlar, D. G. *J. Chem. Phys.* **1991**, *94*, 7875.

(67) Steckler, R.; Hu, W.-P.; Liu, Y.-P.; Lynch, G. C.; Garrett, B. C.; Isaacson A. D.; Lu, D.-h.; Melissas, V.; Truong, T. N.; Rai, S. N.; Hancock, G. C.; Lauderdale, J. G.; Joseph, T.; Truhlar, D. G. POLYRATE version 6.2, University of Minnesota, Minneapolis, 1994 (unpublished).

(68) Hu, W.-P.; Lynch, G. C.; Liu, Y.-P.; Truong, T. N.; Rossi, I.; Stewart, J. J. P.; Steckler, R.; Garrett, B. C.; Isaacson A. D.; Gonzalez-Lafont, A.; Lu, D.-H.; Melissas, V.; Rai, S. N.; Hancock, G. C.; Joseph, T.; Truhlar, D. G. MORATE version 6.2/P6.2-M5.05, University of Minnesota, Minneapolis, 1994 (unpublished).

(69) Lu, D.-H.; Truong, T. N.; Melissas, V.; Lynch, G. C.; Liu, Y.-P.; Garrett, B. C., Steckler, R.; Isaacson, A. D.; Rai, S. N.; Hancock, G. C.; Lauderdale, J. G.; Joseph, T.; Truhlar, D. G. *Comput. Phys. Commun.* **1992**, *71*, 235.

(70) Truong, T. N.; Lu, D.-H.; Lynch, G. C.; Liu, Y.-P.; Melissas, V.; Stewart, J. J. P.; Steckler, R.; Garrett, B. C., Isaacson, A. D.; Gonzalez-Lafont, A.; Rai, S. N.; Hancock, G. C.; Lauderdale, J. G.; Joseph, T.; Truhlar, D. G. *Comput. Phys. Commun.* **1993**, *75*, 143.

(71) *JANAF Thermochemical Tables*, 3rd ed.; Chase, M. W., Jr., Davies, C. A., Downey, J. R., Jr., Frurip, D. J., McDonald, R. A., Syverud, A. N., Eds.; *Natl. Stand. Ref. Data Ser. Vol. 14;* National Bureau of Standards: Washington, DC, 1985.

(72) Benedict, W. S.; Gailor, N.; Plyer, E. K. *J. Chem. Phys.* **1956**, *24*, 2239.

(73) Gibson, S. T.; Greene, J. P.; Berkowitz, J. *J. Chem. Phys.* **1985**, *83*, 4319.

(74) Gurvich, L. V.; Veyts, I. V.; Alcock, C. B. *Thermodynamic Properties of Individual Substances*, 4th ed.; Hemisphere: New York, 1989; Vol. 1.

(75) Carlone, C.; Dalby, F. W. *Can. J. Phys.* **1969**, *47*, 1945.

(76) (a) Schlegel, H. B. *J. Chem. Phys.* **1986**, *84*, 4530. (b) Schlegel, H. B. *J. Phys. Chem.* **1988**, *92*, 3075. (c) McDouall, J. J. W.; Schlegel, H. B. *J. Chem. Phys.* **1990**, *90*, 2363.

(77) Truhlar, D. G. *J. Comput. Chem.* **1991**, *12*, 266.

(78) Gonzalez-Lafont, A.; Truong, T. N.; Truhlar, D. G. *J. Chem. Phys.* **1991**, *95*, 8875.

(79) (a) Garrett, B. C.; Truhlar, D. G.; Magnuson, A. W. *J. Chem. Phys.* **1982**, *76*, 2321. (b) Tucker, S. C.; Truhlar, D. G.; Garrett, B. C.; Isaacson, A. D. *J. Chem. Phys.* **1985**, *82*, 4102. (c) Lu, D.-h.; Maurice, D.; Truhlar, D. G. *J. Am. Chem. Soc.* **1990**, *112*, 6206. (d) Zhao, X. G.; Tucker, S. C.; Truhlar, D. G. *J. Am. Chem. Soc.* **1991**, *113*, 826. (e) Zhao, X. G.; Lu, D.-h.; Liu, Y.-P.; Lynch, G. C.; Truhlar, D. G. *J. Chem. Phys.* **1992**, *97*, 6369. (f) Truhlar, D. G.; Lu, D.-h.; Tucker, S. C.; Zhao, X. G.; Gonzalez-Lafont, A.; Truong, T. N.; Maurice, D.; Liu, Y.-P.; Lynch, G. C. *ACS Symp. Ser.* **1992**, *No. 502*, 16. (g) Hu, W.-P.; Truhlar, D. G. *J. Am. Chem. Soc.* **1994**, *116*, 7797.

JP942157H